

Exploring Charge and Color Breaking vacuum in Non-Holomorphic MSSM

Jyotiranjana Beuria^{a,b} Abhishek Dey^c

^a*Harish-Chandra Research Institute, HBNI, Allahabad 211019, India.*

^b*Regional Centre for Accelerator-based Particle Physics
Harish-Chandra Research Institute, Allahabad 211019, India.*

^c*Maulana Azad College, Government of West Bengal,
8 Rafi Ahmed Kidwai Road, Kolkata 700013, India.*

E-mail: jyotiranjana.beuria@gmail.com, dey.abhishek111@gmail.com

ABSTRACT: Non-Holomorphic MSSM (NHSSM) shows various promising features that are not easily obtained in MSSM. However, the additional Non-Holomorphic (NH) trilinear interactions that attribute to the interesting phenomenological features, also modify the effective scalar potential of the model significantly. We derive analytic constraints involving trilinear parameters A'_t and A'_b that exclude global charge and color breaking minima (CCB). Since the analytic constraints are obtained considering specific directions in the multi-dimensional field space, we further probe the applicability of these constraints by exhaustive scan over NH parameter space with two different regimes of $\tan \beta$ and delineate the nature of metastability by considering vacuum expectation values for third generation squarks. We adhere to a natural scenario by fixing Higgsino mass parameter (μ) to a low value and estimate the allowed ranges of NH trilinear parameters by considering vacuum stability and observed properties of Higgs as the determining criteria.

KEYWORDS: Beyond Standard Model, Supersymmetry Phenomenology

Contents

1	Introduction	1
2	Non-Holomorphic MSSM	3
2.1	CCB in NHSSM	4
2.2	NH parameters and their impact on m_{h_1}	8
3	Results	9
3.1	Nature of the NHSSM scalar potential	10
3.2	CCB minima associated with stop fields	12
3.3	CCB minima associated with sbottom fields	16
3.4	CCB minima associated with both stop and sbottom fields	18
4	Conclusion	21
5	Acknowledgement	23

1 Introduction

The electroweak symmetry breaking (EWSB) and strong interactions are quite successfully explained in the Standard Model (SM) [1] of particle physics. The discovery of the SM-like Higgs boson of mass about 125 GeV at the Large Hadron Collider experiments at ATLAS [2] and CMS [3] marks the end of particle searches within the SM. In such a scenario, studies Beyond the Standard Model (BSM) are motivated by the quest for new physics that is essential for addressing the puzzles that are not resolved in the SM. BSM theories are required to provide a potential solution to the so-called gauge hierarchy problem along with explaining the massive neutrinos and providing suitable particle candidate for Dark Matter (DM) [4–6]. Supersymmetry (SUSY) [7–10] is one of the most widely explored BSM theories. The simplest SUSY extension of the SM, the Minimal Super Symmetric Standard Model (MSSM) addresses many of the issues that are unresolved in the SM.

In the MSSM, the SM fermions and bosons are supplemented by bosonic and fermionic partners transforming under the SM gauge group $SU(3)_C \times SU(2)_L \times U(1)_Y$. As a result, the particle content of the MSSM is significantly enhanced. Apart from the SM particles, squarks (\tilde{q}, \tilde{d}) and sleptons (\tilde{l}) that are charged under $SU(3)_C$ and /or $U(1)_{EM}$ are present

in the MSSM. Additionally, the fermionic counter parts of Higgs bosons and gauge bosons are present in the SUSY model. The color singlet higgsino and the gaugino combine to form charged and neutral mass eigenstates namely the charginos and the neutralinos. The lightest neutralino in a R -parity conserving scenario is a viable particle candidate for a cold dark matter. However, the absence of any hint of SUSY at the LHC has considerably constrained the MSSM. The requirement of large radiative corrections to Higgs boson mass m_{h_1} demands heavier stops or larger stop mixing trilinear soft SUSY breaking parameter (A_t). However, such a large A_t is severely constrained from the $\text{Br}(B \rightarrow X_s + \gamma)$ limits at large $\tan \beta$ [11]. On the other hand, the well-motivated higgsino dark matter that can easily accommodate the relic abundance data from PLANCK [12] and direct detection cross-section measurements from LUX [13] experiment demands the lightest SUSY particle (LSP) to be about 1 TeV. Moreover, the results from Brookhaven experiment [14] for the anomalous magnetic moment of muon or $(g - 2)_\mu$ show about 3σ deviation from the SM predictions creating a scope for a new physics explanation. In the MSSM, a very light smuon ($\tilde{\mu}$) is required to accommodate the $(g - 2)_\mu$ results within 1σ , in a region where the SUSY contribution (a_μ^{SUSY}) [15–21] is dominated by the $\tilde{\mu} - \tilde{\chi}_1^0$ loops. On the contrary, $\tilde{\mu}$ with very low mass is not so friendly with the LHC data [22, 23].

Apart from the experimental and phenomenological aspects, there are a few theoretical issues that need to be explored. In view of current experimental constraints, ElectroWeak Fine Tuning (EWFT) is a major concern in the phenomenological MSSM (pMSSM). In general, larger value of the bilinear Higgs mixing parameter of the superpotential (μ) significantly enhances the EWFT [24]. In the MSSM, even in scenarios that are devoid of any Higgsino like LSP, lower bound on $|\mu|$ is around 100 GeV via LEP limits on lighter chargino. Moreover, in a Higgsino DM setup, relic density limits from PLANCK constrain $m_{\tilde{\chi}_1^0}$ to be $\gtrsim 1$ TeV, that in turn necessitate $|\mu| \sim 1$ TeV enhancing the EWFT significantly.

It has been shown in Refs [25, 26] that extension of the generic MSSM via the inclusion of non-holomorphic (NH) soft SUSY breaking terms, quite satisfactorily ameliorates all the above problems of the MSSM. This extended MSSM, namely the Non-Holomorphic MSSM (NHSSM) has the particle content identical to that of the MSSM, but have extra soft SUSY breaking terms. The NH higgsino mass parameter μ' present in the NHSSM, contributes to the Higgsino content of the neutralinos, but does not have any signature on the tree level neutral scalar potential. The NHSSM can accommodate Higgsino DM even for very low value of μ resulting in the reduction of EWFT [24, 26–28]. The tri-linear NH parameters control the L-R mixing of corresponding squarks and sleptons. Apart from the masses, the L-R mixing effect affects various processes that may be relevant phenomenologically. In this analysis we will focus on the trilinear NH terms for their roles in influencing the scalar potential of the

theory, particularly for the possible appearance of charge and color breaking (CCB) minima [29–42]. Some well-known analytic constraints with simplified assumptions have been used in the MSSM in order to avoid the regions of parameter space where CCB minima is deeper than the desired symmetry breaking (DSB) SM like (SML) vacuum. Consideration of scenarios with global CCB minima, where the DSB minima are stable with respect to tunneling to the deeper CCB minima have led to considerable relaxation of the analytic CCB constraints in the MSSM [43, 44]. If local DSB minimum has a large lifetime in regard to quantum tunneling to global CCB minima, the corresponding DSB minima is referred to as ‘long-lived’ SML vacuum in the literature [45–51]. The long-lived and absolutely stable DSB minima are often collectively referred to as safe vacuum. While exploring the phenomenological features of a model one should consider only those regions of parameter space that are associated with safe vacuum. Besides the above, inclusion of finite temperature effects [51] significantly modifies the vacuum structure further and thus, constraining the allowed region of parameter space with respect to the stability against thermal tunneling. Analyses of vacuum stability considering both thermal and quantum mechanical instabilities have been done in popular models the MSSM [53–57, 60] and the NMSSM [52, 58–60].

In this work, we would probe the vacuum structure of the NHSSM and study the stability of DSB minima using our implementation of complete 1-loop corrected scalar potential in `Mathematica` and the publicly available package `Vevacious` [61] which in turn uses `CosmoTransitions` [62] for determining tunneling time to a deeper vacuum. We would determine the analytic constraints to avoid global CCB vacua using tree-level scalar potential and explore the extent of its applicability. We shall also study the role of different NH parameters in radiative correction to m_{h_1} in order to identify phenomenologically important regions of NH trilinear SUSY breaking parameters associated with third generation squarks sector *viz.* A'_t and A'_b respectively.

The analysis is structured as below. In Sec.2 we very briefly introduce the NHSSM and discuss the analytical CCB constraints and dependence of effective potential on tri-linear NH parameters. We also analyze the role of vacuum expectation values (*vevs*) of stops (\tilde{t}) and sbottoms (\tilde{b}) in determining the fate of the DSB vacuum while satisfying the Higgs mass constraints. In Sec.3 we present the results and analyze them in the light of theoretical predictions. Finally, we conclude in Sec.4.

2 Non-Holomorphic MSSM

Going beyond the generic MSSM, NH SUSY breaking terms potentially fall in the class of terms that may cause hard SUSY breaking [63–70], particularly in models with singlet scalars.

The “may be soft” [64] D-term contributions like $\frac{1}{M^3}[XX^*\Phi^2\Phi^*]_D$ and $\frac{1}{M^3}[XX^*D^\alpha\Phi D_\alpha\Phi]_D$ give rise to the NH terms in the Lagrangian *viz.* $\phi^2\phi^*$ and $\psi\psi$ respectively. Here X and Φ are chiral superfields and SUSY breaking in the hidden sector is driven by *vev* of an auxiliary field F belonging to X . We note that $\langle F \rangle / M$ should refer to a weak scale mass which we consider here as the W-boson mass M_W . However, in models like pMSSM it can be varied independently. Hence, coefficients of $\phi^2\phi^*$ and $\psi\psi$ varies as $\frac{|\langle F \rangle|^2}{M^3} \sim \frac{M_W^2}{M}$. Thus, it is evident that they are highly suppressed in super-gravity type of models. However, in weak scale scenario $\phi^2\phi^*$ and $\psi\psi$ are quite significant and appear as the NH trilinear terms and bare Higgsino mass term respectively ¹.

This was discussed or at least pointed out in several works [64–66, 68, 71–75]. Impact of NH parameters on m_{h_1} , electroweak fine tuning, $\text{Br}(B \rightarrow X_s + \gamma)$ and $(g - 2)_\mu$ have been analyzed in Ref.[26]. Earlier works involving the analysis of the effects of NH terms include Ref.[76–78]. Here we would like to explore the scalar potential of NHSSM with emphasis on the vacuum stability issues. Our prime focus will be on the attribution of the NH terms towards determining the fate of the EWSB vacuum.

2.1 CCB in NHSSM

We remind that the MSSM is considered to have only holomorphic soft SUSY breaking terms. The trilinear soft terms, in particular, are given by as follows [8].

$$-\mathcal{L}_{soft} \supset \tilde{Q} \cdot H_u y_t A_t \tilde{U} + \tilde{Q} \cdot H_d y_b A_b \tilde{D} + \tilde{L} \cdot H_d y_\tau A_\tau \tilde{E} + h.c. \quad (2.1)$$

We have only shown here the dominant terms involving the third generation of sfermions. It has been shown that in the absence of any gauge singlet it is possible to extend the SUSY breaking soft sector by including NH soft SUSY breaking terms, without aggravating any quadratic divergence [63, 66, 72]. Thus, the NH soft terms of the NHSSM in general that include trilinear coupling terms as well as a NH higgsino mass (μ') term are given by [25, 75]

$$-\mathcal{L}'_{soft} \supset \tilde{Q} \cdot H_d^c y_t A_t' \tilde{U} + \tilde{Q} \cdot H_u^c y_b A_b' \tilde{D} + \tilde{L} \cdot H_u^c y_\tau A_\tau' \tilde{E} + \mu' \tilde{H}_u \cdot \tilde{H}_d + h.c. \quad (2.2)$$

Thus, the scalar potential at the tree level including the Higgs and the stop fields read as follows.

$$\begin{aligned} V|_{\text{tree}} = & m_2^2 H_u^2 + m_1^2 H_d^2 + m_{\tilde{t}_L}^2 \tilde{t}_L^2 + m_{\tilde{t}_R}^2 \tilde{t}_R^2 - 2B_\mu H_d H_u + 2y_t A_t H_u \tilde{t}_R \tilde{t}_L \\ & - 2y_t (\mu + A_t') \tilde{t}_L \tilde{t}_R H_d + y_t^2 (H_u^2 \tilde{t}_L^2 + H_u^2 \tilde{t}_R^2 + \tilde{t}_R^2 \tilde{t}_L^2) + \frac{g_1^2}{8} (H_u^2 - H_d^2 + \frac{\tilde{t}_L^2}{3} - \frac{4\tilde{t}_R^2}{3})^2 \\ & + \frac{g_2^2}{8} (H_u^2 - H_d^2 - \tilde{t}_L^2)^2 + \frac{g_3^2}{6} (\tilde{t}_L^2 - \tilde{t}_R^2)^2, \end{aligned} \quad (2.3)$$

¹For details discussion see Ref.[26] and references therein.

where $m_2^2 = m_{H_u}^2 + \mu^2$ and $m_1^2 = m_{H_d}^2 + \mu^2$ and $m_{H_u}^2$ ($m_{H_d}^2$) is the soft squared mass term for up (down) type Higgs. Relevant terms may be added to the above equation to construct the complete scalar potential at the tree level taking into account the other sfermions. In the above expression, vanishing value of A'_t leads to the generic MSSM scenario. In this analysis we will explore the CCB constraints at tree-level for deriving simple analytic result. The results from our numerical scans are obtained via **Vevacious** [61] which includes 1-loop corrected potential both at zero temperature and finite temperature. Furthermore, in presence of CCB minima, it computes the tunneling rate from DSB vacuum to the former using **CosmoTransitions** [62]. However, we consider the scalar potential only at the tree-level in order to obtain the analytic CCB constraints analogous to those used in the MSSM. One loop correction (in the \overline{DR} -scheme) [79, 80]) at zero temperature is given by

$$\Delta V_{\text{rad.corr.}} = \sum_i \frac{n_i}{64\pi^2} m_i^4 \left(\ln \frac{m_i^2}{Q^2} - \frac{3}{2} \right), \quad (2.4)$$

where the sum runs over all real scalars, vectors and Weyl fermions that are present in the model with

$$n_i = (-1)^{2s_i} (2s_i + 1) Q_i C_i \quad (2.5)$$

and $Q_i = 2(1)$ for charged particles (neutral particles), C_i is the color degrees of freedom, s_i is the spin of the particle, m_i is the mass of the same and Q is the renormalization scale used.

The stability of the DSB vacuum can be significantly affected by thermal corrections to the scalar potential. The 1-loop thermal correction to the potential at temperature ‘T’ is given by [81]

$$\Delta V_{\text{thermal}} = \frac{1}{2\pi^2} \sum T^4 J_{\pm} (m^2/T^2), \quad (2.6)$$

where

$$J_{\pm}(r) = \pm \int_0^{\infty} dx \, x^2 \ln(1 \mp e^{-\sqrt{x^2+r}}). \quad (2.7)$$

The sum in equation 2.6 runs over all degrees of freedom that couple to the scalar fields including the scalar fields themselves. J_+ (J_-) corresponds to the corrections arising from bosons (Weyl fermions) and m is the mass of the corresponding particle at zero temperature. $J_{\pm}(\frac{m^2}{T^2})$ asymptotically approaches zero ($-\infty$) as $\frac{m^2}{T^2}$ approaches ∞ (zero). It is to noted that thermal corrections would always lower the potential [54, 61] depending on the magnitude of $\frac{m^2}{T^2}$. The complete scalar potential at one loop that includes both zero temperature and thermal corrections, is given by

$$V = V|_{\text{tree}} + \Delta V_{\text{rad.corr.}} + \Delta V_{\text{thermal}} \quad . \quad (2.8)$$

Analytic CCB constraints in MSSM were derived along particular direction of field space, namely “D-flat” direction [29]. Keeping this in mind, we consider non vanishing *vevs* for the two higgs scalar and the stops fields. The latter are responsible for the generation of CCB minima. In the direction where $|H_d| = |H_u| = |\tilde{t}_R| = |\tilde{t}_L| = \zeta$, the scalar potential (Eq.2.3) reduces to

$$\mathbf{V}_{\text{tree}} = a\zeta^4 + b\zeta^3 + c\zeta^2, \quad (2.9)$$

where $a = \left(3y_t^2 - \frac{g_1^2 + g_2^2}{8}\right)$, $b = [2y_t A_t - 2y_t(\mu + A'_t)]$ and $c = (m_1^2 + m_2^2 + m_{\tilde{t}_R}^2 + m_{\tilde{t}_L}^2 - 2B_\mu)$. Minimizing the above potential with respect to ζ and considering non-vanishing ζ , we obtain $4a\zeta^2 + 3b\zeta + 2c = 0$.

Hence, the value of the field at the minima is

$$\zeta = \frac{-3b \pm \sqrt{9b^2 - 32ac}}{8a}. \quad (2.10)$$

From the reality condition of the roots, we get $9b^2 > 32ac$. $V_{\min} > 0$ at the minima implies, $a\zeta^2 + b\zeta + c > 0$. Here we consider a scenario with 4 *vevs* otherwise, the contribution of A'_t and A_t cannot be taken into account simultaneously. One may also consider the scalar potential excluding the holomorphic trilinear terms in a three *vevs* scenario with non vanishing *vevs* for H_d , \tilde{t}_R and \tilde{t}_L with $H_u = 0$. Nevertheless, A_t plays a very crucial role in providing adequate m_{h_1} . Besides, both the Higgs fields have non-vanishing *vevs* in phenomenologically viable region of MSSM. As a result for any realistic scenario in MSSM and beyond one has $H_d \neq 0$ and $H_u \neq 0$. This necessitates the consideration of non-zero *vevs* for H_d and H_u . Using the reality condition for the ζ at the minima, in simplified scenario with $H_d = 0$ [44] we obtain

$$A_t^2 > 2.67(m_2^2 + m_{\tilde{t}_L}^2 + m_{\tilde{t}_R}^2), \quad (2.11)$$

where $m_2^2 = m_{H_u}^2 + \mu^2$. This is referred as the condition for the existence of a deeper CCB in MSSM which is often approximated as

$$A_t^2 > 3(m_2^2 + m_{\tilde{t}_L}^2 + m_{\tilde{t}_R}^2), \quad (2.12)$$

that is the traditionally used CCB constraint associated with stop (\tilde{t}) scalars receiving *vevs* [29, 30, 32–35, 39, 41]. Similar constraints are used for different sfermion fields. In NHSSM, we consider the following inequality resulting from reality condition $9b^2 > 32ac$ that implies

$$9 \times 4y_t^2 [A_t - (\mu + A'_t)]^2 > 32 \left\{ 3y_t^2 - \frac{g_1^2 + g_2^2}{8} \right\} (m_1^2 + m_2^2 + m_{\tilde{t}_L}^2 + m_{\tilde{t}_R}^2 - 2B_\mu). \quad (2.13)$$

In contrast to MSSM, here we do analyze the scalar potential considering non-vanishing $v_{\tilde{e}vs}$ for all the four scalar fields. The Eq.2.13 simplifies to

$$[A_t - (\mu + A'_t)]^2 > 3 \left\{ 1 - \frac{g_1^2 + g_2^2}{24y_t^2} \right\} (m_1^2 + m_2^2 + m_{\tilde{t}_L}^2 + m_{\tilde{t}_R}^2 - 2B_\mu). \quad (2.14)$$

Eq.2.14 identifies regions of parameter space associated with global CCB minima. Neglecting the contributions from g_1^2 and g_2^2 with respect to y_t^2 , the CCB constraint in NHSSM for \tilde{t} fields becomes

$$[A_t - (\mu + A'_t)]^2 < 3 (m_1^2 + m_2^2 + m_{\tilde{t}_L}^2 + m_{\tilde{t}_R}^2 - 2B_\mu). \quad (2.15)$$

One can always retrieve the traditional constraint in MSSM (Eq.2.12) from Eq.2.15 assuming $A'_t = 0$ and $H_d = 0$. As discussed in Ref.[29], the most stringent CCB constraint is obtained when the relative sign between the trilinear terms in the potential are always considered positive. Thus, in NHSSM the analytic condition predicting an absolutely stable DSB vacuum is

$$\{|A_t| + |\mu| + |A'_t|\}^2 < 3 (m_1^2 + m_2^2 + m_{\tilde{t}_L}^2 + m_{\tilde{t}_R}^2 - 2B_\mu). \quad (2.16)$$

Along with the absolute stable DSB minima, we also consider long-lived DSB minima, in presence of global CCB vacuum that in turn will increase the valid parameter space. Here one should note that rate of tunneling from DSB false vacuum to such CCB true vacuum is roughly proportional to e^{-a/y^2} , where a is a constant of suitable dimension that can be determined via field theoretic calculations and y is the Yukawa coupling. The tunneling rate is enhanced for large Yukawa couplings [30, 47–51]. As a result, the third generation of sfermions will be the most important candidate in connection with the presence of potentially dangerous global minima. In models like the MSSM and the NHSSM, the Yukawa couplings vary with $\tan \beta$ which is given by $\tan \beta = \frac{v_u}{v_d}$. However, unless $\tan \beta$ is very large the relation $y_t > y_b > y_\tau$ is by and large satisfied, consistent with the mass hierarchy of the corresponding fermions. Hence, global CCB minima associated with \tilde{t} fields will be most dangerous due to comparatively larger y_t . The \tilde{b} fields may also play an important role in determining the fate of the DSB minima. A large value of the NH parameter A'_b associated with \tilde{b} significantly modifies m_{h_1} and \tilde{b} phenomenology particularly for large $\tan \beta$. In the phenomenologically interesting regions of parameter space, the structure of the scalar potential is modified by the presence of large A'_b and in such a setup, vacuum stability needs to be re-explored. In this context, one should study the analytic CCB constraint associated with the \tilde{b} fields. Following a similar method as adopted for \tilde{t} , one gets the CCB constraint for \tilde{b} to be

$$\{|A_b| + |\mu| + |A'_b|\}^2 < 3 \left\{ 1 - \frac{g_1^2 + g_2^2}{24y_b^2} \right\} (m_1^2 + m_2^2 + m_{\tilde{b}_L}^2 + m_{\tilde{b}_R}^2 - 2B_\mu). \quad (2.17)$$

Unlike the case of \tilde{t} , here we cannot neglect g_1 and g_2 with respect to y_b , since y_b is not very large. In the limit of MSSM, in three *vevs* scenario with non-vanishing *vevs* for H_d , \tilde{b}_L and \tilde{b}_R , with $H_u = 0$, we get the well-known CCB constraint for \tilde{b} , namely

$$A_b^2 < 3(m_1^2 + m_{\tilde{b}_L}^2 + m_{\tilde{b}_R}^2), \quad (2.18)$$

directly from the Eq.2.17. As pointed out earlier the terms associated with g_1 and g_2 contribute to the potential in the direction where all the *vevs* are equal only if all the four *vevs* are non-vanishing. Thus, they naturally do not appear in the traditional CCB constraints, that are essentially derived in a simple three *vev* setup. Similar analysis may be done for $\tilde{\tau}$ fields. However, we focus only on the effect of considering \tilde{t} and \tilde{b} *vevs*, since y_τ is small. At this point, before going for a detailed numerical study we try to estimate the limitations of the analytically derived CCB constraints of NHSSM namely Eqs.2.16 and 2.17. First, the contributions of the \tilde{t} and \tilde{b} fields are considered separately. On the other hand, in a realistic scenario they jointly affect the vacuum structure of the model. Secondly, only the direction where equal *vevs* are attributed to all the fields is taken into account. Thirdly, in a phenomenological analysis of the pMSSM, $\tan \beta$ varies over a wide range. Thus, y_t and y_b vary and g_1 and g_2 may not be always negligible with respect to Yukawa couplings. Lastly, this work goes beyond an absolute vacuum stability by accommodating long-lived scenarios, demanding a detail numerical analysis. In our work using **Vevacious** [61] we probe the vacuum structure to find the DSB minima. We explore a four *vev* scenario considering non-vanishing *vevs* for \tilde{t}_L, \tilde{t}_R along with H_d and H_u . In the other part of our analysis we consider a different four *vev* combination involving $\tilde{b}_L, \tilde{b}_R, H_d$ and H_u , in order to gauge the role of \tilde{b} fields in determining the fate of the DSB minima. In both the above cases, we try to estimate the applicability of the analytic constraints. Finally, we analyze a more involved scenario with six *vevs* where non-zero *vevs* were attributed to \tilde{b}_L and \tilde{b}_R along with $\tilde{t}_L, \tilde{t}_R, H_d$ and H_u . Additionally, a varying $\tan \beta$, changes the values of v_u and v_d that in turn modify the yukawa couplings. The vacuum structure thus depends on $\tan \beta$. We consider two different zones of $\tan \beta$ to explore the dependency.

2.2 NH parameters and their impact on m_{h_1}

Besides affecting vacuum stability, the NH trilinear parameters play a significant role in phenomenology where left-right mixing of sfermions are important. Additionally, the NH higgsino mass parameter μ' is important in processes dominated by higgsino and it controls the overall higgsino phenomenology. The NH parameters significantly modify the $\text{Br}(B \rightarrow X_s + \gamma)$ and radiative corrections to m_{h_1} . The role of A'_t together with μ' in the radiative corrections of m_{h_1} has been studied in Ref.[26] in the low scale NHSSM (pNHSSM). Here we

would like to probe the contribution of the NH parameters towards the radiative corrections to m_{h_1} in order to identify phenomenologically interesting regions of NH parameters for exploring vacuum stability. The radiative correction to m_{h_1} due to stop-loop is given by

$$\Delta m_{h,top}^2 = \frac{3g_2^2 \bar{m}_t^4}{8\pi^2 M_W^2} \left[\ln \left(\frac{m_{\tilde{t}_1} m_{\tilde{t}_2}}{\bar{m}_t^2} \right) + \frac{X_t^2}{m_{\tilde{t}_1} m_{\tilde{t}_2}} \left(1 - \frac{X_t^2}{12 m_{\tilde{t}_1} m_{\tilde{t}_2}} \right) \right]. \quad (2.19)$$

Here $X_t = A_t - (\mu + A'_t) \cot \beta$ and \bar{m}_t stands for the running top-quark mass that includes electroweak, QCD and SUSY QCD corrections [82]. Apart from this, particularly for large $\tan \beta$, A'_b the NH trilinear soft parameter associated with the bottom squarks, has significant bearing on m_{h_1} . The contribution from sbottom-loop is

$$\Delta m_{h,bottom}^2 = \frac{3g_2^2 \bar{m}_b^4}{8\pi^2 M_W^2} \left[\ln \left(\frac{m_{\tilde{b}_1} m_{\tilde{b}_2}}{\bar{m}_b^2} \right) + \frac{X_b^2}{m_{\tilde{b}_1} m_{\tilde{b}_2}} \left(1 - \frac{X_b^2}{12 m_{\tilde{b}_1} m_{\tilde{b}_2}} \right) \right], \quad (2.20)$$

where $X_b = A_b - (\mu + A'_b) \tan \beta$ ². In the MSSM, the contribution from \tilde{b} loops is important only for large $\tan \beta$ and μ , since \bar{m}_b is significantly smaller than \bar{m}_t . Hence, in a MSSM scenario motivated by low EWFT, where μ is predominantly very small, the contribution to m_{h_1} due to the \tilde{b} is negligible, although the effect is $\tan \beta$ enhanced. The situation is quite different in the NHSSM. Here for a large value of A'_b , $\Delta m_{h,bottom}^2$ is albeit small but not negligible compared to $\Delta m_{h,top}^2$ because of the associated $\tan \beta$ enhancement. Thus even in a scenario motivated by low EWFT, the radiative correction to m_{h_1} from \tilde{b} loops can be non-negligible in the NHSSM. However, the contribution may be negative or positive depending on the value of X_b .

3 Results

We explore the nature of the scalar potential in a semi-analytic approach that demonstrates the dependency on NH parameters. We study the degree of applicability of the analytic CCB constraints *viz.* Eqs. 2.16 and 2.17 in the NHSSM. Considering the contributions of A'_t and A'_b to m_{h_1} , we analyze the stability of the DSB minima using **Vevacious** [61]. **SARAH** [83–86] and **SPheno** [87–91] were used for model building and spectrum generation respectively. The spectra generated by **SPheno** include complete two-loop corrections to Higgs mass even from NH parameters [92, 93]. The numerical study is performed in three different set-ups of non-vanishing *vevs*. First, we exclusively probe the stability of DSB minima in presence of global CCB minima associated with non-zero *vevs* of \tilde{t}_L and \tilde{t}_R . Here, we consider a four-*vev* scenario with non-zero *vevs* for H_d , H_u , \tilde{t}_L and \tilde{t}_R . Then, we explore the role of

²A similar result for the stau contribution would involve $X_\tau = A_\tau - (\mu + A'_\tau) \tan \beta$.

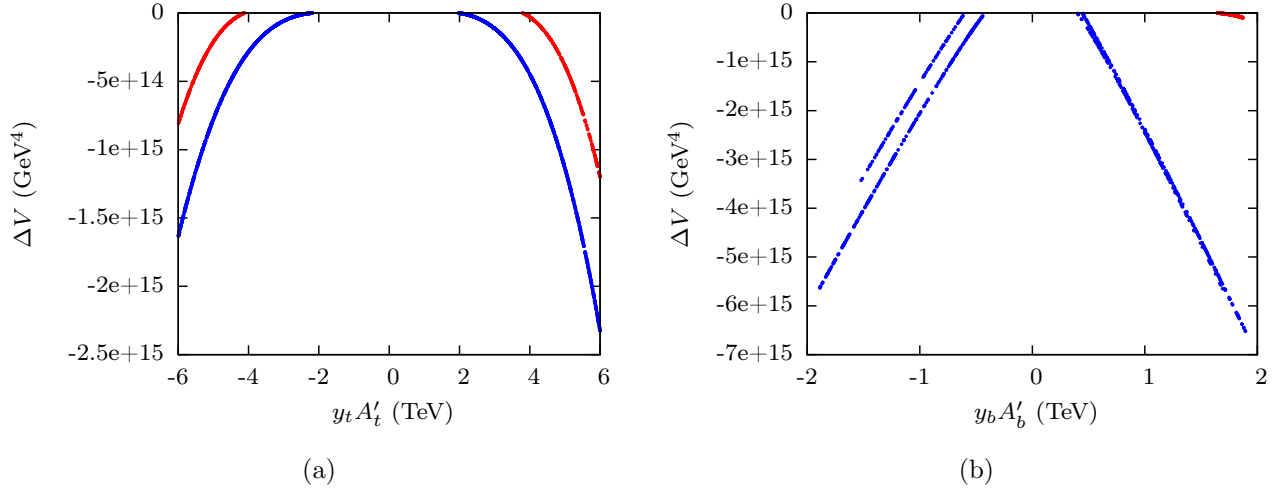


Figure 1. ΔV represents the depth of the potential at the deeper CCB vacuum with respect to the field origin. Fig.1(a) shows the variation of ΔV with $y_t A'_t$ for \tilde{t} vevs scenario. Fig.1(b) depicts the $y_b A'_b$ dependence of ΔV for \tilde{b} vevs scenario. The red and blue points correspond to $\tan \beta = 50$ and $\tan \beta = 5$ respectively. Lowering of the potential depending on the suitable values of A'_t and A'_b is evident from the above plots. Large $|A'_t|$ and $|A'_b|$ thus essentially can lower the potential depending on the given choices of the other pMSSM parameters that are kept fixed.

\tilde{b}_L and \tilde{b}_R in rendering the DSB minima unstable. Finally, we analyze a combined multiple-*vevs* scenario with non-vanishing *vevs* for six scalar fields viz. H_d , H_u , \tilde{t}_L , \tilde{t}_R , \tilde{b}_L and \tilde{b}_R . y_t and y_b will significantly affect the vacuum stability against CCB minima. Hence, we divide our analysis into two $\tan \beta$ regimes, viz. $5 \leq \tan \beta \leq 10$ and $40 \leq \tan \beta \leq 50$.

3.1 Nature of the NHSSM scalar potential

Now we focus on the NH parameter space to identify the nature of CCB vacuum in detail, by assigning *vevs* to \tilde{t} and \tilde{b} fields separately. This is essential in order to identify the dangerous directions in the field space while studying the role A'_t and A'_b in modifying the vacuum structure of the model. Since pNHSSM is principally motivated by naturalness, we choose $\mu = 200$ GeV for the entire analysis. Fig.1 demonstrates the variation of ΔV with the NH trilinear parameters for the vacuum deeper than the DSB one, where ΔV represents the depth of the scalar potential with respect to the origin. Fig.1(a) (1(b)) corresponds to the \tilde{t} (\tilde{b}) *vevs* scenario. The red (blue) color refers to $\tan \beta = 50$ ($\tan \beta = 5$). We keep $m_{\tilde{t}_L}$, $m_{\tilde{t}_R}$ and $m_{\tilde{b}_R}$ fixed at 2 TeV. The MSSM trilinear term $y_t A_t$ ($y_b A_b$) is fixed at 2 TeV (0). The soft parameter B_μ in Eq.2.3 is kept fixed at 2×10^5 GeV². The relevant NH parameters³

³In SPheno convention, the input trilinear soft SUSY breaking terms for sfermions are $y_f A_f$.

for the scenarios with \tilde{t} and \tilde{b} *vevs* are given by the following ranges.

$$\begin{aligned} -6 \text{ TeV} &\leq y_t A'_t \leq 6 \text{ TeV} \\ -2 \text{ TeV} &\leq y_b A'_b \leq 2 \text{ TeV}. \end{aligned} \quad (3.1)$$

A'_t and A'_b clearly play a significant role in lowering the scalar potential. It is to be noted further, that the range of $y_b A'_b$ is kept small. This is because large A'_b leads to very large SUSY threshold corrections to bottom yukawa coupling and thus, the spectrum generator **SPheno** aptly reports error. Recently, the effect of such corrections to y_b has been studied in the context of vacuum stability in the MSSM [55, 56]. For the given choice of parameters, the depth of the DSB vacuum is many orders shallower than the depth at the deeper CCB vacuum. Furthermore, we observe from Fig.1(a) and 1(b) that depth of the potential at the CCB vacuum is deeper for $\tan \beta = 5$ case. Stop sector being the major contributor to the effective potential ($y_t A_t = 2 \text{ TeV}$ gives large contribution even for vanishingly small NH parameters), the effect gets enhanced for $\tan \beta = 5$ compared to $\tan \beta = 50$ due to large y_t for the former case. We also observe from Fig.1(a) and 1(b) that the depth of the potential at $\tan \beta = 5$ for the case with \tilde{b} *vev* is a bit deeper compared to the \tilde{t} *vev* one. This is due to the additional contribution arising from sbottom sector for large A'_b in the \tilde{b} case.

It is to be noted in Fig.1(b) that there are two distinct blue lines for $A'_b < 0$. This is purely a numerical artifact due to the fact that the minimization routine **Minuit** used in **Vevacious** sometimes misses out some of the minima during random scan. Thus, in some cases, it reports a different CCB vacuum for similar parameter sets. In the framework of **Vevacious**, the *vevs* are bounded by a hypercube of length $20Q$. We keep the renormalization scale Q at a value $\sqrt{m_{\tilde{t}_L} m_{\tilde{t}_R}}$ all through this work.

In the Eqns. 2.16 and 2.17 for the constraints on non-holomorphic parameters, all the *vevs* are considered to be equal. However, this is not a realistic scenario. In Fig.2(a) and Fig.2(b), we present schematic representation of contours for the cases for stop and sbottom *vevs* respectively. The fixed parameters are given as follows.

$$y_t A_t = 2 \text{ TeV}, \mu = 200 \text{ GeV}, m_{\tilde{t}_L} = 1 \text{ TeV}, m_{\tilde{t}_R} = 2 \text{ TeV}, m_{\tilde{b}_R} = 1 \text{ TeV}. \quad (3.2)$$

While studying the effect of stop fields, we choose $y_t A'_t = -3600 \text{ GeV}$ with vanishing A'_b . On the other hand for the scenario with sbottom *vevs*, $y_b A'_b$ is kept at 800 GeV with vanishing A'_t . The encircled closed contours surround the minima of the potential. The central contour encloses the DSB minima, while the other two contours that encircle regions with non-zero *vevs* for stops (sbottoms) represent CCB minima. For the stop *vevs* (Fig.2(a)), we choose $H_u^0 = H_d^0$ direction and for the sbottom *vev* (Fig.2(b)), we choose $H_d^0 = 0$ direction in order to capture the global CCB minima and the DSB vacuum. In the subsequent sub-sections,

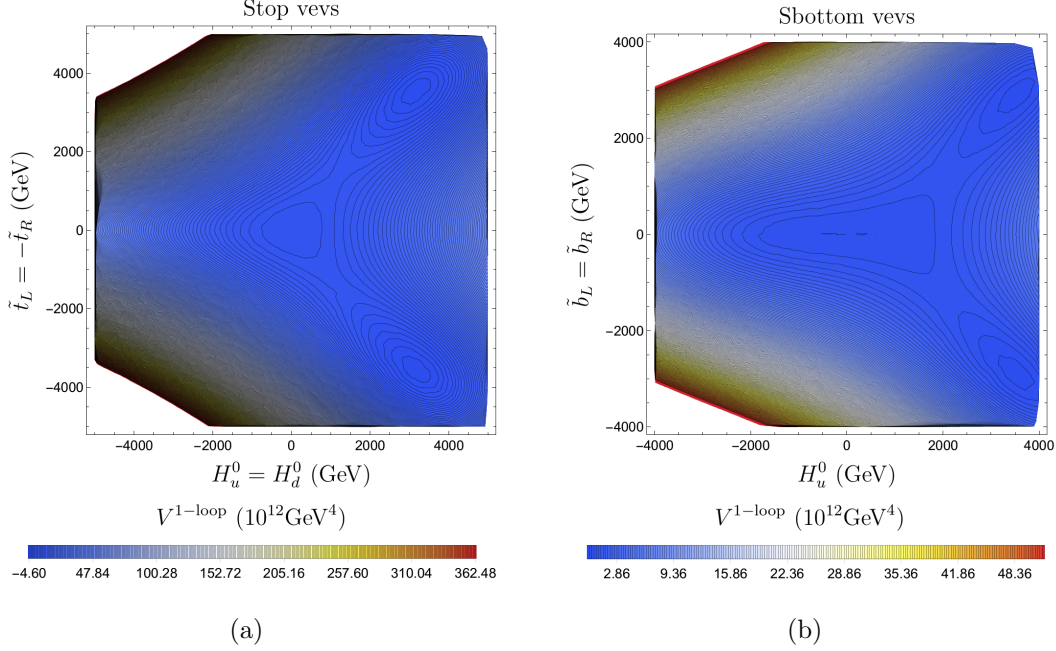


Figure 2. The encircled closed contours surround the minima of the potential. The central contour encloses the DSB minima, while the other two contours that encircle regions with non-zero vevs for stops (sbottoms) in Fig. 2(a) (2(b)) represent the global CCB minima.

we analyze the CCB vacua due to stop fields, sbottom fields and finally, combination of both stop and sbottom fields on a broader region of parameter space compared to the one presented above.

3.2 CCB minima associated with stop fields

Keeping an eye on Eq. 2.16 we define $\mathcal{M}_t^2 = [m_1^2 + m_2^2 + m_{t_L}^2 + m_{t_R}^2 - 2B_\mu]$ and $\widetilde{A}_t^2 = (|A_t| + |\mu| + |A'_t|)^2$. These variables will play a crucial role in determining the applicability of the analytic constraint of Eq. 2.16. We also define similar variables $\mathcal{M}_b^2 = (m_1^2 + m_2^2 + m_{t_L}^2 + m_{b_R}^2 - 2B_\mu)$ and $\widetilde{A}_b^2 = (|A_b| + |\mu| + |A'_b|)^2$ to be used while studying the CCB constraints arising out of non-vanishing vevs of \tilde{b} fields.

We probe the vacuum stability of the model for both smaller ($5 \leq \tan \beta \leq 10$) and larger values ($40 \leq \tan \beta \leq 50$) of $\tan \beta$. We analyze in a minimal four-vev set-up considering non-zero vevs for the Higgs and the stops. We vary the relevant parameters in the following

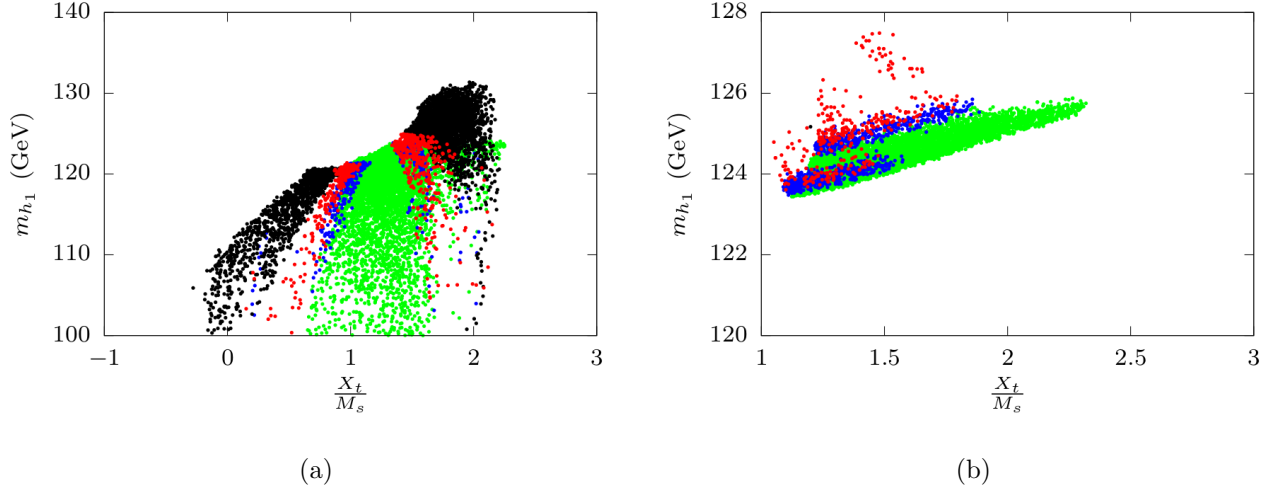


Figure 3. The vacuum stability profile is plotted in $\frac{X_t}{M_s} - m_{h_1}$ plane, where $X_t = A_t - (\mu + A'_t) \cot \beta$ and $M_s = \sqrt{m_{\tilde{t}_1} m_{\tilde{t}_2}}$ with tree level stop masses. The left (right) plot corresponds to $5 \leq \tan \beta \leq 10$ ($40 \leq \tan \beta \leq 50$). Green and blue regions correspond to stable and long-lived vacuum respectively. The red (black) points refer to thermally excluded (quantum mechanically unstable) vacuum.

ranges.

$$\begin{aligned}
-1 \text{ TeV} &\leq \mu' \leq 1 \text{ TeV} \\
-6 \text{ TeV} &\leq y_t A'_t \leq 6 \text{ TeV} \\
500 \text{ GeV} &\leq m_{\tilde{t}_L} \leq 2 \text{ TeV}.
\end{aligned} \tag{3.3}$$

We keep $y_t A_t$ fixed at 2 TeV, and set all other holomorphic soft trilinear parameters to zero. All scalar mass parameters excluding $m_{\tilde{t}_L}$ are fixed at 2 TeV. Since we study the vacuum structure with specific motive of investigating the role of NH parameters, we do not scan over holomorphic trilinear parameters. Other fixed parameters are same as that of Fig.1(a). Fig.3 shows the vacuum stability profile in $X_t - m_{h_1}$ plane. In spite of having no influence on vacuum stability, μ' is scanned over a moderate range. This is due to the fact that it contributes to m_{h_1} via chargino loop [94, 95]. The green and blue points are associated with stable and long-lived DSB minima. They are collectively referred to as safe vacua. The black and the red colored regions are excluded since the DSB minima associated with them are rendered unstable with respect to quantum tunneling to deeper CCB minima and thermal effects respectively. Fig.3(a) and 3(b) correspond to low and high $\tan \beta$ regimes. In Fig.3(a), we see stable points (green) cluster around $\frac{X_t}{M_s} \approx 1$ with close by metastable points. This is mainly because of the choice of $y_t A_t = 2$ TeV with $\mu = 200$ GeV. Thus, most of the points appear on positive side of $\frac{X_t}{M_s}$. The vacuum stability profile for the MSSM [54]

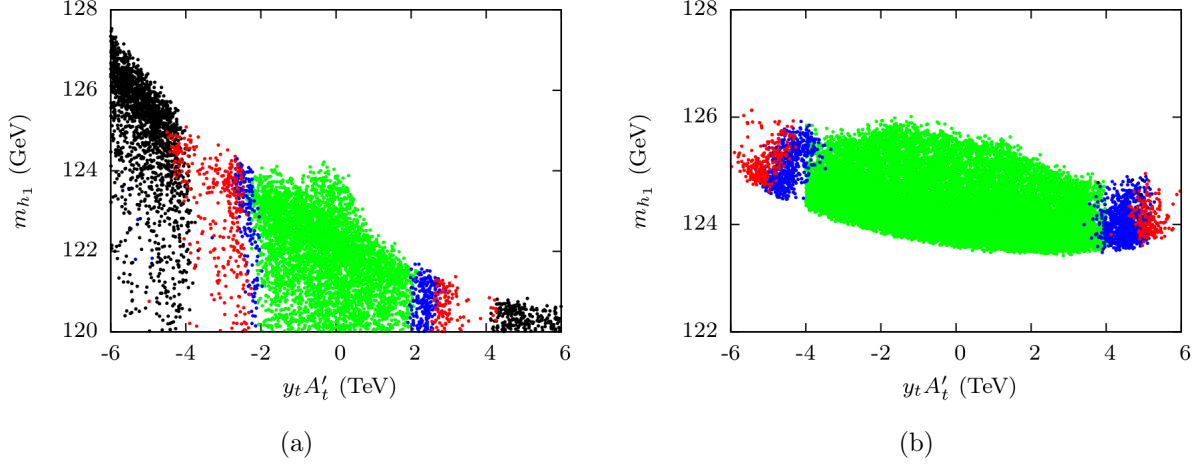


Figure 4. The stability profile of DSB minima in $y_t A'_t - m_{h_1}$ plane corresponding to the scan of Eq.3.3. Figs.4(a) and 4(b) corresponds to $(5 < \tan \beta < 10)$ and $(40 < \tan \beta < 50)$ respectively. The color codes are same as that for Fig.3.

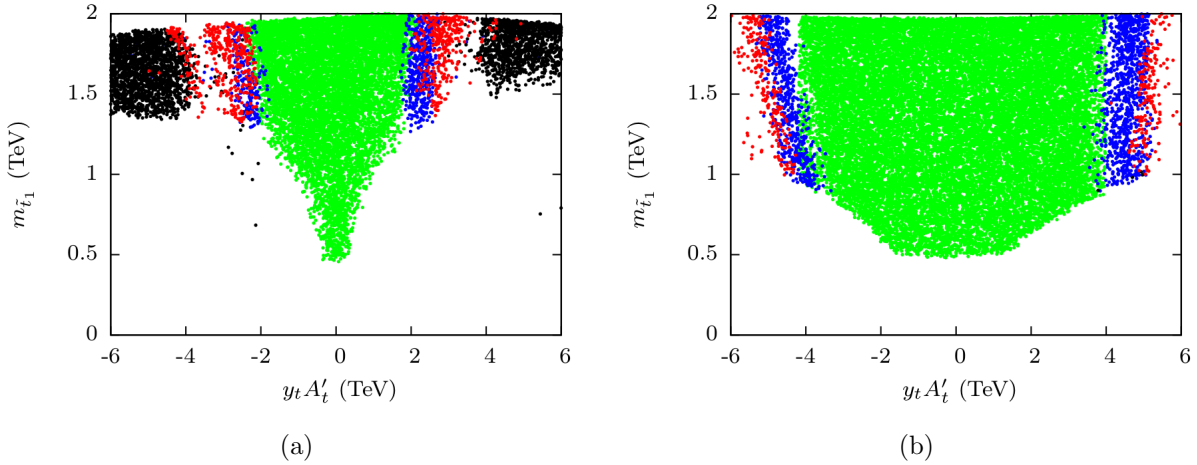


Figure 5. The stability profile of the DSB minima in $y_t A'_t - m_{\tilde{t}_1}$ plane corresponding to the scan of Eq.3.3. Figs.5(a) and 5(b) corresponds to $(5 < \tan \beta < 10)$ and $(40 < \tan \beta < 50)$ respectively. The color codes are same as that for Fig.3.

in $X_t - m_{h_1}$ plane is qualitatively very much similar to Fig.3(a). Fig.3(b) appear to be a bit different from Fig.3(a). This is because mass of the Higgs boson gets boosted for chosen value of $y_t A_t$ (2 TeV) and $\tan \beta = 50$. There are no quantum mechanically short-lived points (black) for Fig.3(b), whereas there are large number of black points in Fig.3(a).

Fig.4 shows the dependence of m_{h_1} on the $y_t A'_t$ for $\tan \beta$ scanned over two different domains. Fig.4(a) shows the stability profile for $5 \leq \tan \beta \leq 10$. The spread of m_{h_1} for

particular value of $y_t A'_t$ is due to the effect of variation of $m_{\tilde{t}_L}$ and $\tan\beta$ on the radiative corrections arising out of stop loops (Eq. 2.19). Fig.4(b) shows the similar plot for $40 \leq \tan\beta \leq 50$. As discussed in Sec.2, A'_t contribution in the radiative correction to m_{h_1} via \tilde{t} loop is $\tan\beta$ suppressed. As a result the effect of $y_t A'_t$ on m_{h_1} is more prominent in low $\tan\beta$ region. Thus, for Fig.4(b) we see that the variation of m_{h_1} is significantly small compared to Fig.4(a). In both the plots, the central region characterized by comparatively lower $|y_t A'_t|$ is associated with stable DSB vacua, whereas large $|y_t A'_t|$ region is associated with unsafe DSB minima. In between the two regions, there exists a small zone associated with long-lived states (blue). We find that for low $\tan\beta$ and $|y_t A'_t| \gtrsim 3$ TeV the DSB minima becomes unsafe and they are excluded via quantum tunneling or thermal effects. On the contrary, for $40 \leq \tan\beta \leq 50$, comparatively large values of $|y_t A'_t|$ (< 4 TeV), is allowed in the region of parameter space associated with safe vacuum. This is due to the fact that the term in the potential associated with A'_t is suppressed for large $\tan\beta$.

Fig.5 shows the vacuum stability profile in $y_t A'_t - m_{\tilde{t}_1}$ plane for same set of scans. As before, Fig.5(a) (Fig.5(b)) represents the case with $5 \leq \tan\beta \leq 10$ ($40 \leq \tan\beta \leq 50$). We observe from both the plots that $m_{\tilde{t}_1}$ could be rather large in the region of metastability triggered by large $|y_t A'_t|$. We have kept $m_{\tilde{t}_R}$ fixed at 2 TeV. Hence large $m_{\tilde{t}_L}$ along with large $|y_t A'_t|$ facilitate the appearance of deeper CCB vacua by inducing large mixing between \tilde{t}_L and \tilde{t}_R . Thus, $m_{\tilde{t}_1}$ becomes large for large $|y_t A'_t|$. We also notice that due to $\tan\beta$ suppression, the spread of green points in Fig.5(b) is more compared to Fig.5(a). Furthermore, the flat green edge ($m_{\tilde{t}_L} \approx m_{\tilde{t}_1} \approx 500$ GeV) is also broader compared to Fig.5(a) for the same reason.

Fig.6 shows the stability profile with m_{h_1} along y -axis and the relevant factor $\frac{\tilde{A}_t^2}{\mathcal{M}_t^2}$ (see Eq.2.16) along the x -axis. Here, we explore the applicability of the analytic CCB constraints in the NHSSM, exclusively in four *vevs* scenario with non-vanishing *vevs* for stops and Higgs fields. The variable in the horizontal axis is predicted to be less than 3 for stable DSB minima according to Eq. 2.16. It appears that such constraint holds quite reliably for the chosen region of parameter space. However, since the analytic constraint of Eq. 2.16 was derived under the consideration of stable vacua only, the constraint may be relaxed in the present scenario where, we also include long-lived DSB minima as viable vacua of the theory. This is evident from the extent of the long-lived states in the region where $3 \lesssim \frac{\tilde{A}_t^2}{\mathcal{M}_t^2} \lesssim 4$. We observe that the safe vacua spread over a wider range of $\frac{\tilde{A}_t^2}{\mathcal{M}_t^2}$ for large $\tan\beta$. This is quite expected as the contribution of A'_t is $\tan\beta$ suppressed. Moreover for large $\tan\beta$, y_t being comparatively smaller, the rate of quantum tunneling is decreased enhancing the presence of long-lived vacua over a wider range of $y_t A'_t$ and $\frac{\tilde{A}_t^2}{\mathcal{M}_t^2}$. In the next section, a study of the deeper CCB vacua arising from the *vevs* of the sbottoms is presented.

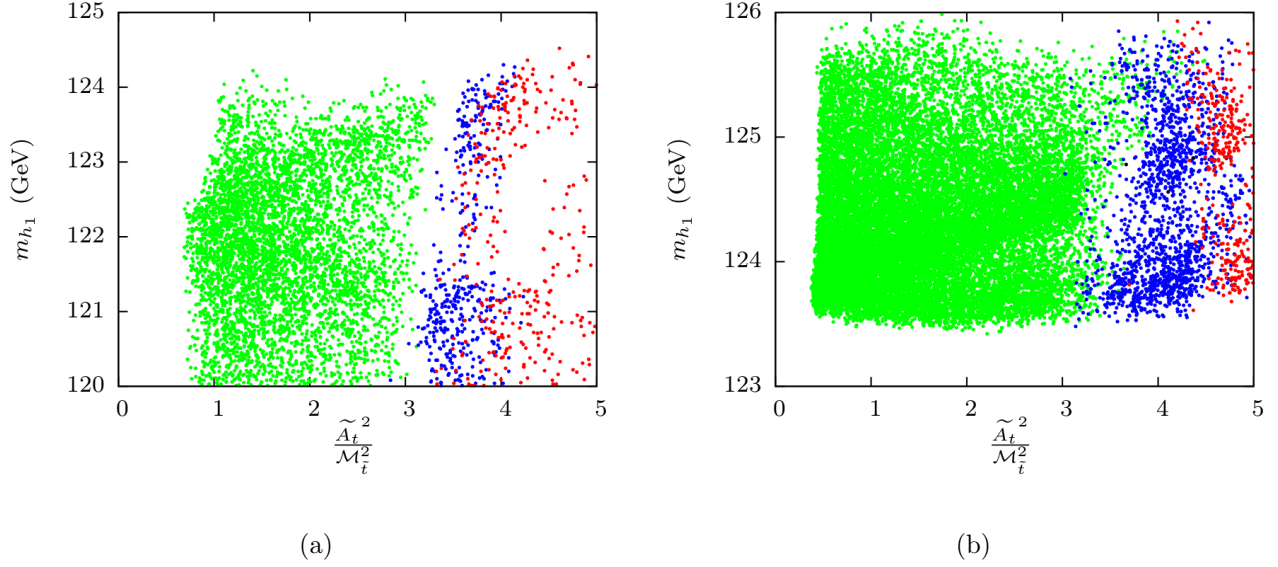


Figure 6. The stability profile of the DSB vacuum in the $\frac{\tilde{A}_t^2}{\mathcal{M}_{\tilde{t}}^2} - m_{h_1}$ plane. Fig.6(a) (6(b)) refers to $5 \leq \tan \beta \leq 10$ ($40 \leq \tan \beta \leq 50$). The color codes are same as that for fig.3.

3.3 CCB minima associated with sbottom fields

As discussed in Sec.2 the global CCB minima associated with \tilde{t} fields are more dangerous with respect to the tunneling rate due to large yukawa coupling (y_t). The \tilde{b} fields may also become important particularly for large $\tan \beta$. Hence, in this section, we study the role of $y_b A'_b$ associated with \tilde{b}_L and \tilde{b}_R in determining the fate of DSB minima. We probe the vacuum stability of the model for both smaller ($5 \leq \tan \beta \leq 10$) and larger values ($40 \leq \tan \beta \leq 50$) of $\tan \beta$. Considering the effects on vacuum stability, we vary the relevant parameters in the following ranges.

$$\begin{aligned}
-1 \text{ TeV} &\leq \mu' \leq 1 \text{ TeV} \\
-2 \text{ TeV} &\leq y_b A'_b \leq 2 \text{ TeV} \\
500 \text{ GeV} &\leq m_{\tilde{t}_L} \leq 2 \text{ TeV} \\
500 \text{ GeV} &\leq m_{\tilde{b}_R} \leq 2 \text{ TeV}
\end{aligned} \tag{3.4}$$

We keep $y_t A_t$ fixed at 2 TeV, and set all other holomorphic soft trilinear parameters to zero. All scalar mass parameters excluding $m_{\tilde{t}_L}$ and $m_{\tilde{b}_R}$ are fixed at 2 TeV. Fig.7(a) shows the stability profile in $y_b A'_b - m_{h_1}$ plane for low $\tan \beta$ ($5 < \tan \beta < 10$). As expected, we see that the DSB minima are safe for most of the values of A'_b . This is consistent with the discussion in Sec.2, as for small $\tan \beta$ the NH terms associated with \tilde{b} are less dominant. It appears

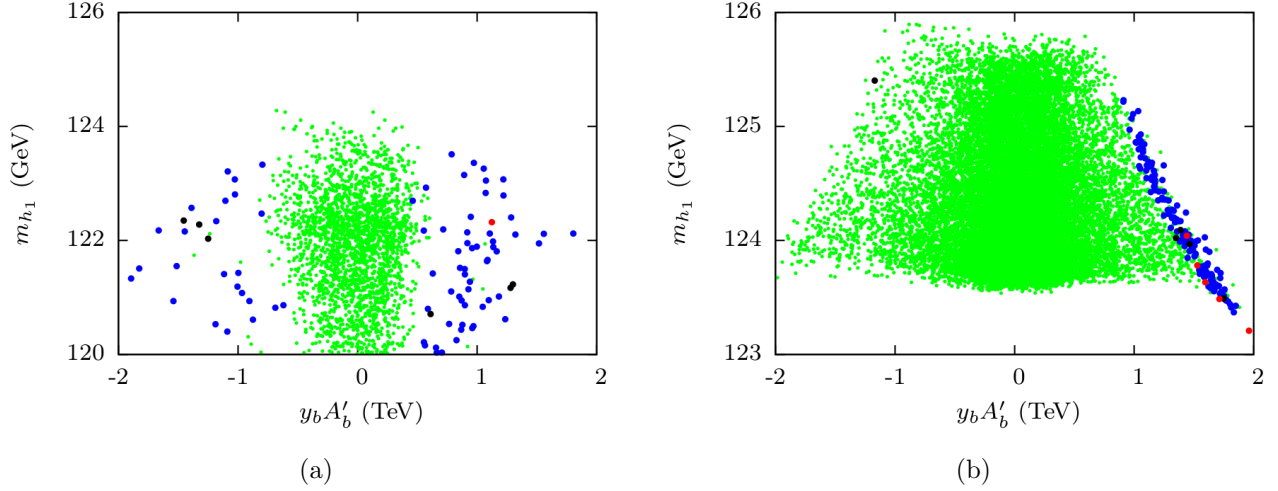


Figure 7. *Fig.7(a) shows the stability profile in $y_b A'_b - m_{h_1}$ plane for $5 < \tan \beta < 10$ corresponding to scan of Eq.3.4. Fig.7(b) is a similar plot for $40 < \tan \beta < 50$. The color codes for stability profile is same as that for Fig.3.*

that most of the metastable points are actually long-lived and thus, these are considered safe. For low $\tan \beta$, y_b is very small and mixing between \tilde{b}_L and \tilde{b}_R would only be enhanced if difference between $m_{\tilde{t}_L}$ and $m_{\tilde{b}_R}$ is rather small. Hence the long-lived (blue) points have small difference between $m_{\tilde{t}_L}$ and $m_{\tilde{b}_R}$.

Fig.7(b) shows the stability profile for large $\tan \beta$. Here we see that large values of $y_b A'_b > 0$ have deeper CCB vacua compared to the corresponding DSB ones. The region $y_b A'_b < 0$ hardly appear to possess metastable points. This is because the SUSY threshold corrections to y_b for the chosen value of $\mu = 200$ GeV increases y_b very significantly for $A'_b < 0$ compared to $A'_b > 0$. Thus, a particle mass spectrum calculated by **SPheno** contains a DSB vacuum consistent at two-loop level. The model parameters deduced at this setup may not necessarily yield a similar DSB vacuum when one-loop correction to scalar potential is employed. This makes **Vevacious** reassign the input vacuum to a rolled down vacuum configuration other than the DSB one determined from the spectrum file. In our analysis, we are not considering such kind of particle spectra where two-loop corrections change the structure of the potential very significantly. This results in hardly any metastable points for $A'_b < 0$. We further notice that m_{h_1} spreads over a larger range for large $\tan \beta$. This is due to the fact that the contribution of $|A'_b|$ to m_{h_1} is enhanced by $\tan \beta$ (Eq.2.20).

In Fig.8, we plot the stability profile in $\frac{\tilde{A}_b^2}{\tilde{M}_b^2} - m_{h_1}$ plane. Fig.8(a) (Fig.8(b)) corresponds to small (large) $\tan \beta$. For both $\tan \beta$ regimes, the analytic constraint seems to be unnecessary since almost all of the region of parameter space that was scanned over, corresponds

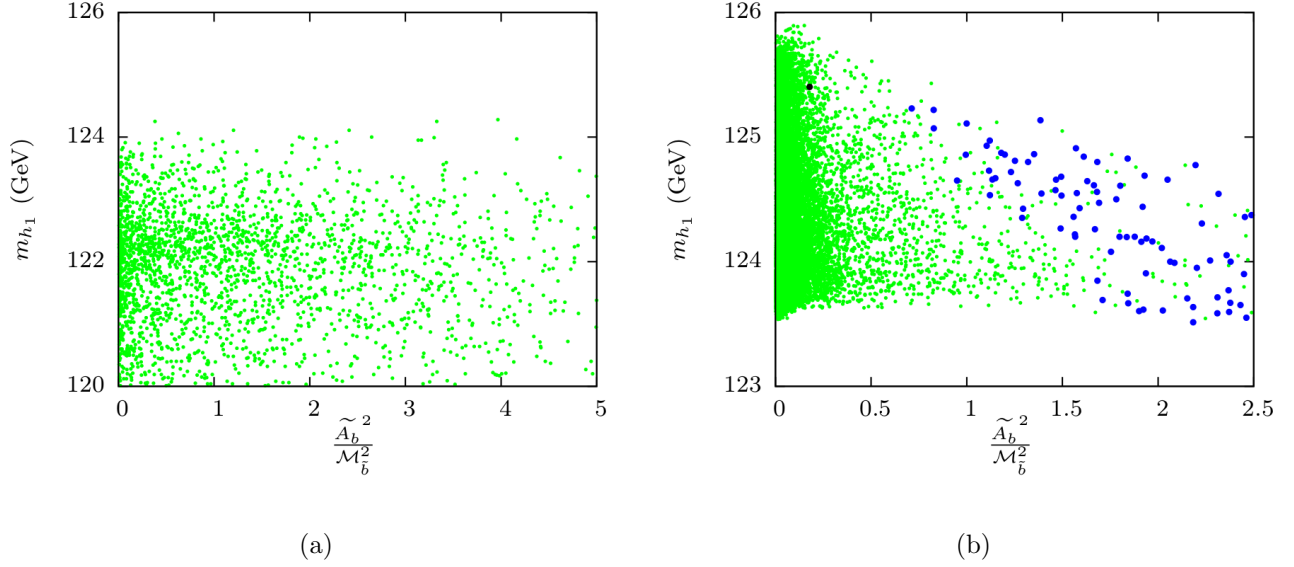


Figure 8. *Fig.8(a)* shows the stability profile in $\frac{\tilde{A}_b^2}{\mathcal{M}_b^2} - m_{h1}$ plane for $5 < \tan \beta < 10$. *Fig.8(b)* is similar plot for $40 < \tan \beta < 50$. The color codes for stability profile is same as that for Fig.4. It is evident from the plots that the analytic expression regarding CCB constraint Eq.2.17 is unimportant for small $\tan \beta$, unlike the case of large $\tan \beta$ (see text for details).

to stable or long-lived vacua. For large $\tan \beta$, stable vacuum corresponds to region with rather smaller values of $\frac{\tilde{A}_b^2}{\mathcal{M}_b^2}$ compared to the case with smaller $\tan \beta$. For smaller $\tan \beta$, the metastable points appearing in Fig.7(a) do not appear for $\frac{\tilde{A}_b^2}{\mathcal{M}_b^2} < 5$. On the other hand, the metastable points appearing in Fig.7(b) appear for smaller values of $\frac{\tilde{A}_b^2}{\mathcal{M}_b^2}$. This is because for smaller $\tan \beta$, y_b is very small compared to the case with larger $\tan \beta$. This renders A'_b very large for smaller $\tan \beta$ for a particular value of $y_b A'_b$ compared to larger $\tan \beta$. Considering absolute stable vacua, we observe that metastability appears even when $\frac{\tilde{A}_b^2}{\mathcal{M}_b^2}$ is significantly less than 3 on contrary to what predicted by Eq.2.17. This is due to the wide variation of y_b in the large $\tan \beta$ regime. Hence $\frac{g_1^2 + g_2^2}{24y_b^2}$ is not always negligible with respect to 1. Thus, the factor 3 does not arise.

3.4 CCB minima associated with both stop and sbottom fields

In this section we study a more involved scenario characterized by the non-vanishing *vevs* for all the third generation squark fields along with Higgs fields. We vary the relevant parameters in the following ranges.

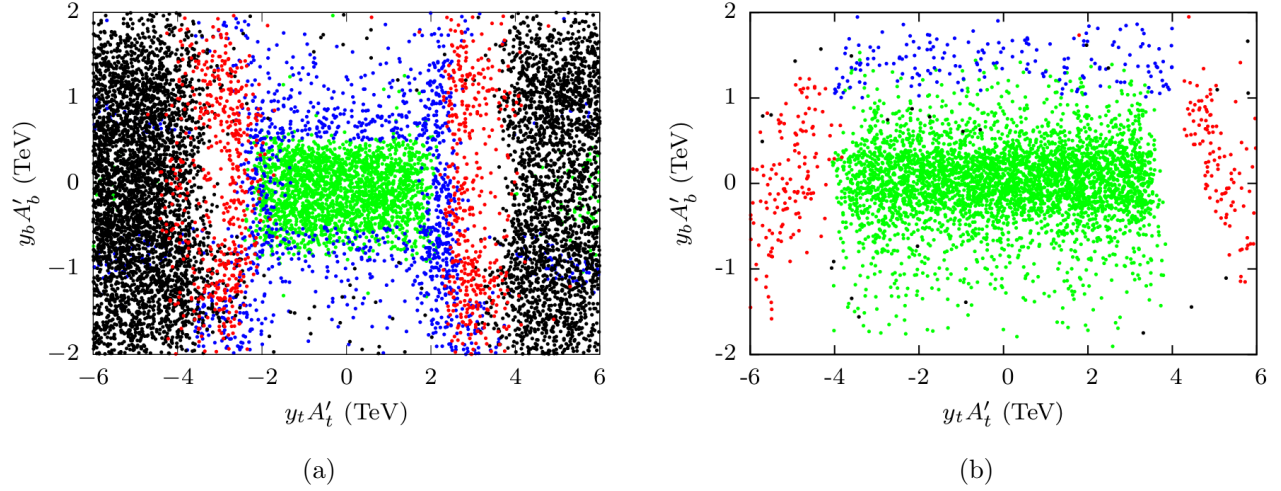


Figure 9. Figs.9(a) and 9(b) classify by the parameter points according to the fate of DSB minima associated with them, in the $y_t A'_t - y_b A'_b$ plane, for low and high regime of $\tan \beta$. Fig.9 corresponds to the scan of Eq.3.5. It is evident that the effect of A'_t is more prominent for low $\tan \beta$, whereas A'_b plays a crucial role for large $\tan \beta$.

$$\begin{aligned}
-1 \text{ TeV} &\leq \mu' \leq 1 \text{ TeV}, \\
-6 \text{ TeV} &\leq y_t A'_t \leq 6 \text{ TeV}, \\
-2 \text{ TeV} &\leq y_b A'_b \leq 2 \text{ TeV}, \\
500 \text{ GeV} &\leq m_{\tilde{t}_L} \leq 2 \text{ TeV}, \\
500 \text{ GeV} &\leq m_{\tilde{b}_R} \leq 2 \text{ TeV}.
\end{aligned} \tag{3.5}$$

We keep $y_t A_t$ fixed at 2 TeV and μ at 200 GeV. All sfermion mass parameters except $m_{\tilde{t}_L}$ and $m_{\tilde{b}_R}$, are fixed at 2 TeV. Fig.9 shows the stability profile in the $y_t A'_t - y_b A'_b$ plane. The color codes for stability profile are same as that for Fig.3. Fig.9(a) and 9(b) correspond to low and high $\tan \beta$ regimes respectively. It is evident from Fig.9(a) that for low $\tan \beta$, the effect of A'_b towards determining the fate of the DSB vacuum is negligible and the vacuum stability is primarily determined by A'_t . This is consistent with the discussion of the scalar potential of NHSSM (see Sec.2). Both the plots identify a central region near $A'_t = 0 = A'_b$. This region is associated with absolute stable DSB vacuum, shown in green in the plots. Bordering the green central region, there exists a small zone associated with long-lived DSB minima⁴. Beyond that, there exist regions characterized by DSB vacua that are rendered

⁴In some cases, **Vevacious** fails to determine the fate of the DSB vacuum when thermal corrections to the effective potential is switched on. Without thermal corrections, these regions appear as long-lived in our scan.

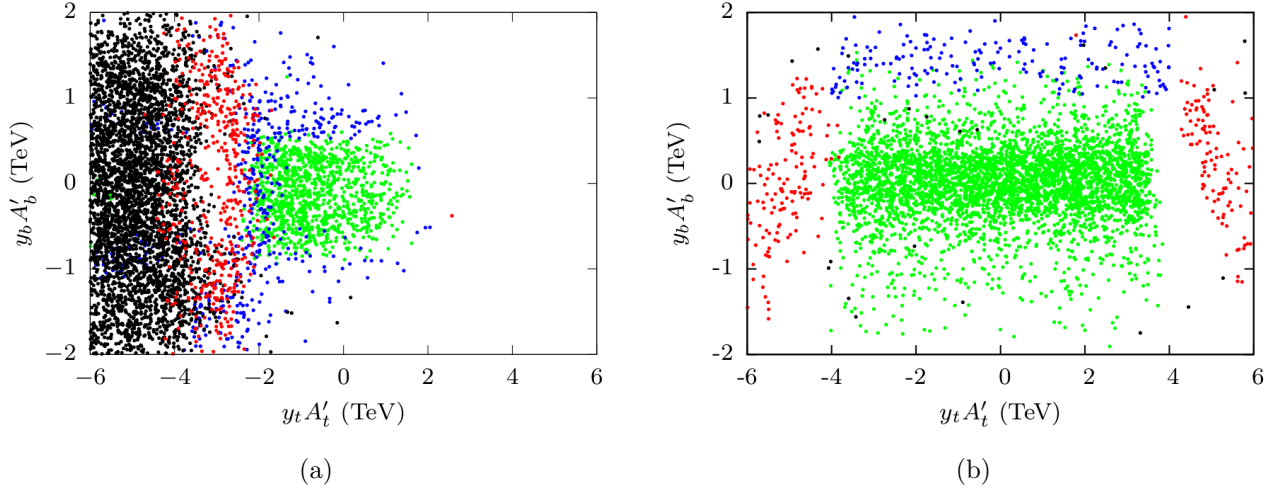


Figure 10. Figs.10(a) and 10(b) are same as Fig.9 with the limits on m_{h_1} imposed. It is evident that the region with $y_t A'_t > 2$ TeV is excluded via limits on m_{h_1} for low $\tan \beta$.

unstable via quantum tunneling or thermal effects. Despite the similarity in the nature of the two plots, there are some striking differences that arise due to the two different ranges of $\tan \beta$ that are considered in our analysis. Fig.9(a) constrains $|y_t A'_t|$ to be within 2.0 TeV for stable points, whereas there is almost no restriction imposed on $y_b A'_b$ when safe vacua (both stable and long-lived points) are considered. Fig.9(b) reveals that the stable points can appear for wider range of $|y_t A'_t|$ compared to that in the low $\tan \beta$ limit, since its effect is more prominent for low $\tan \beta$. Thus, the zone $|y_t A'_t| < 4$ TeV is easily accommodated in the model. Demanding absolute stability one requires $|y_b A'_b| \lesssim 1.5$ TeV, however, that may be relaxed by a small amount via inclusion of long-lived states. We further notice that the metastability of the DSB vacuum is mostly governed by large $y_t A'_t$. However, there are metastable points (mostly long-lived) even for smaller $y_t A'_t$. The origin of such metastable points is attributed to sbottom *vevs*.

Now we impose the experimental limits for m_{h_1} while considering a 3 GeV window resulting into the following range [96–102].

$$122.1 \text{ GeV} \leq m_{h_1} \leq 128.1 \text{ GeV}. \quad (3.6)$$

The above uncertainty essentially arises from scale dependence, problems in computing higher order loop and renormalization scheme related dependencies. Imposing the above constraint of Eq.3.6 on Fig.9, results into Fig.10. Fig.10(a) shows that a large region of parameter space associated with $y_t A'_t > 2$ TeV is excluded via the limits on m_{h_1} . As expected, A'_t plays a significant role in the radiative corrections to m_{h_1} for low $\tan \beta$. For large $\tan \beta$,

as shown in Fig.10(b), A'_b is also important in regard to vacuum stability but the radiative corrections to m_{h_1} keeps it well within the range of Eq.3.6. This is consistent with the results obtained from fig.7(b).

4 Conclusion

Even after the first few years of running of the LHC, SUSY signal is yet to be observed. This has severely constrained many models of low scale SUSY including the MSSM. In the post Higgs@125 GeV era, the requirement of the lighter SM like Higgs boson of the MSSM to have a mass of $m_{h_1} \sim 125$ GeV translates into the need of large radiative corrections. This on the other hand, necessitates heavier stop squark sector or large stop mixing trilinear soft parameter (A_t). At the same time, LHCb results on B-physics processes like $\text{Br}(B \rightarrow X_s + \gamma)$ further constrain the allowed parameter space of the model especially for large $\tan \beta$. Regarding the DM perspective, a bino like DM requires a strong correlation among unrelated SUSY parameters to provide with the proper relic abundance. A wino like DM, consistent with PLANCK data, on the other hand, demands the LSP to be extremely heavy (> 2 TeV). A higgsino like DM does not require correlation between unrelated SUSY parameters and is able to satisfy the relic density limits for a relatively lower mass ($\mu \sim 1$ TeV). However, a large μ leads to a significant enhancement of EWFT. The Non-Holomorphic MSSM (NHSSM) is one of the simplest extensions of the MSSM that can significantly or at least partially ameliorate all of the above mentioned problems. The NHSSM is constructed via inclusion of non-holomorphic (NH) SUSY breaking soft trilinear interactions with the coefficients A'_t, A'_b etc. along with a NH higgsino mass soft parameter (μ'). In this model, A'_t and to some extent A'_b contribute to the radiative corrections to m_{h_1} arising out of the stop and sbottom loops. Hence, comparatively smaller values of stop squarks or $|A_t|$ can satisfy the higgs mass data. B-physics constraints are also more easily satisfied through left-right mixing in the stop sector. The higgsino mass in the NHSSM is governed by $|\mu - \mu'|$, whereas EWFT has no μ' dependence at the tree-level. As a result, a higgsino like DM that provides required amount of relic abundance is obtained even for a lower value of μ . Thus, electroweak scale naturalness is comfortably restored in the NHSSM. Although the higgs scalar potential is identical to that of the MSSM, the full scalar potential that includes the squarks and sleptons, is modified by the presence of NH trilinear parameters. ' μ' ' on the other hand has no effect on the scalar potential at the tree level. The presence of charged and colored scalars may give rise to global charge and color breaking (CCB) minima. This is a well known problem and studied widely in literature for models like the MSSM and the NMSSM. Analytic constraints are often used to exclude the presence of global CCB

minima in the MSSM. These constraints consider absolute stability of the Desired Symmetry Breaking (DSB) minima and confine the allowed ranges of A_t and A_b . Consideration of a quantum mechanically as well as thermally stable DSB vacua in presence of a global CCB minima extends the allowed parameter space significantly. These long-lived states along with the absolute stable ones are collectively referred to as safe vacua. Since the analytic constraints are usually derived under highly simplified assumptions and are based on the choice of directions within the multi-dimensional field space, numerical analysis is required for precise understanding of the vacuum stability over the parameter space. In this work, we first study the analytic and numerical ways of imposing the CCB constraints and study the vacuum stability by including the possibility of having long-lived states.

In the first part, we derive the analytic CCB constraints in the NHSSM. Non-vanishing *vevs* are attributed to the Higgs and stop fields while deriving the CCB constraints involving stop fields. On the other hand, Higgs and sbottom fields were considered to have non-zero *vevs* while deriving the CCB relations in a scenario where the charge and color breaking is caused by the sbottom fields. In a simplified scenario, all the non-vanishing *vevs* are considered to be equal while deriving the analytic expressions that constrain A'_t and A'_b for assuring the absolute stability of the DSB minima. However, these analytic constraints have limitations since the assumption of equality of *vevs* is hardly a reality in a SUSY model. Thus, the dependence on $\tan\beta$ becomes quite important. Furthermore, the analytic constraints would not be sufficient once one includes cosmologically long-lived state.

Along with the theoretical analysis, we follow a semi-analytic approach using complete 1-loop corrected effective potential implemented via **Mathematica** to investigate the influence of the NH terms on the scalar potential of the model. We find that, the terms associated with A'_t and A'_b effectively lower the scalar potential of the model. This lowering essentially leads to the appearance of global CCB minima depending on the values of the NH parameters. We also present an exhaustive scan over relevant region of parameter space by using the dedicated package **Vevacious** that includes both zero temperature effects and finite temperature corrections to the NHSSM potential.

We divide our **Vevacious** based analysis into three different parts depending on the fields whose *vevs* are allowed to be non-vanishing. First, in order to probe the effect of the stop fields, non-vanishing *vevs* are attributed to stops and higgs fields. The effect of A'_t is more prominent for low $\tan\beta$, where the former is confined in a quite small range via the requirement of safe vacua. On the other hand, for large $\tan\beta$, a comparatively wider range of A'_t is allowed. This is due to the fact, that the contribution of A'_t in the scalar potential is $\tan\beta$ suppressed. The region of parameter space with adequate value of m_{h_1} , is associated with both safe and dangerous vacua. m_{h_1} becomes important in a CCB related study, simply

because a right zone of mass of the higgs boson require large values of trilinear parameters A_t and A'_t that are sensitive to CCB analyses. The results obtained from **Vevacious** based analysis show the presence of a significant region of long-lived states. Hence the region of parameter space having safe vacua can be extended considerably which is otherwise ruled out by analytical CCB constraint.

Exploring the model for CCB minima associated with the sbottom fields, we find that the CCB constraint is hardly effective in constraining A'_b for small values of $\tan \beta$. For large $\tan \beta$, there are long-lived states even if the analytical CCB constraint is satisfied. We also find that most of the region is safe against deeper CCB vacua arising from sbottom *vevs*.

In a more realistic scenario, stop and sbottom fields together modify the scalar potential. In order to probe this effect, all the third generation squarks along with the higgs fields are assumed to have non-vanishing *vevs*. We try to locate the safe vacuum in the $y_t A'_t - y_b A'_b$ plane. The origin ($A'_t = A'_b = 0$) corresponds to the MSSM scenario where the NH terms are absent. There exists a region of absolute stable vacuum around $A'_t = 0 = A'_b$. This zone is bounded by regions that are characterized by the presence of long-lived DSB minima. Beyond this, almost the entire $y_t A'_t - y_b A'_b$ plane is excluded due to the instability of DSB minima. A wider range of $y_t A'_t$ is allowed for large $\tan \beta$, but it is confined in a quite smaller range for low $\tan \beta$. Moreover, the allowed range of m_{h_1} has visible impact for the case with low $\tan \beta$ and $A'_t > 0$. On the other hand, most of the region with large $\tan \beta$ is consistent with such a range.

5 Acknowledgement

AD would like to thank Indian Association for the Cultivation of Science for infrastructural support. JB is partially supported by funding available from the Department of Atomic Energy, Government of India for the Regional Centre for Accelerator-based Particle Physics (RECAPP), Harish-Chandra Research Institute. JB is also partially supported by the ‘INFOSYS scholarship for senior students’. The authors acknowledge AseshKrishna Datta and Utpal Chattopadhyay for their useful comments and encouragement. The authors also acknowledge the use of the cluster computing setup available at the High-Performance Computing facility of HRI.

References

- [1] E. S. Abers and B. W. Lee, Phys. Rept. **9**, 1 (1973); A. Sirlin, Nucl. Phys. B **196**, 83 (1982); T. P. Cheng and L. F. Li, Oxford, Uk: Clarendon (1984) 536 P. (Oxford Science Publications); A. Djouadi, Phys. Rept. **457**, 1 (2008) [hep-ph/0503172].

- [2] G. Aad *et al.* [ATLAS Collaboration], Phys. Lett. B **716**, 1 (2012) [arXiv:1207.7214 [hep-ex]].
- [3] S. Chatrchyan *et al.* [CMS Collaboration], Phys. Lett. B **716**, 30 (2012) [arXiv:1207.7235 [hep-ex]]; S. Chatrchyan *et al.* [CMS Collaboration], JHEP **1306**, 081 (2013) [arXiv:1303.4571 [hep-ex]].
- [4] G. Jungman, M. Kamionkowski and K. Griest, Phys. Rept. **267**, 195 (1996) doi:10.1016/0370-1573(95)00058-5 [hep-ph/9506380].
- [5] G. Bertone, D. Hooper and J. Silk, Phys. Rept. **405**, 279 (2005) doi:10.1016/j.physrep.2004.08.031 [hep-ph/0404175].
- [6] K. Garrett and G. Duda, Adv. Astron. **2011**, 968283 (2011) doi:10.1155/2011/968283 [arXiv:1006.2483 [hep-ph]].
- [7] For reviews on supersymmetry, see, e.g., H. P. Nilles, Phys. Rep. **110**, 1 (1984); J. D. Lykken, hep-th/9612114; J. Wess and J. Bagger, *Supersymmetry and Supergravity*, 2nd ed., (Princeton, 1991).
- [8] M. Drees, P. Roy and R. M. Godbole, *Theory and Phenomenology of Sparticles*, (World Scientific, Singapore, 2005).
- [9] H. Baer and X. Tata, *Weak scale supersymmetry: From superfields to scattering events*, Cambridge, UK: Univ. Pr. (2006) 537 p.
- [10] D. J. H. Chung, L. L. Everett, G. L. Kane, S. F. King, J. D. Lykken and L. T. Wang, Phys. Rept. **407**, 1 (2005); H. E. Haber and G. Kane, Phys. Rep. **117**, 75 (1985) ; S. P. Martin, arXiv:hep-ph/9709356.
- [11] U. Haisch and F. Mahmoudi, JHEP **1301**, 061 (2013) doi:10.1007/JHEP01(2013)061 [arXiv:1210.7806 [hep-ph]].
- [12] P. A. R. Ade *et al.* [Planck Collaboration], Astron. Astrophys. **571**, A16 (2014) doi:10.1051/0004-6361/201321591 [arXiv:1303.5076 [astro-ph.CO]].
- [13] D. S. Akerib *et al.* [LUX Collaboration], Phys. Rev. Lett. **112**, 091303 (2014) doi:10.1103/PhysRevLett.112.091303 [arXiv:1310.8214 [astro-ph.CO]].
- [14] G. W. Bennett *et al.* [Muon g-2 Collaboration], Phys. Rev. D **73**, 072003 (2006) doi:10.1103/PhysRevD.73.072003 [hep-ex/0602035].
- [15] K. Kowalska, L. Roszkowski, E. M. Sessolo and A. J. Williams, JHEP **1506**, 020 (2015) doi:10.1007/JHEP06(2015)020 [arXiv:1503.08219 [hep-ph]].
- [16] S. Heinemeyer, D. Stockinger and G. Weiglein, Nucl. Phys. B **690**, 62 (2004) doi:10.1016/j.nuclphysb.2004.04.017 [hep-ph/0312264].
- [17] U. Chattopadhyay, D. K. Ghosh and S. Roy, Phys. Rev. D **62**, 115001 (2000) doi:10.1103/PhysRevD.62.115001 [hep-ph/0006049].

- [18] T. Moroi, Phys. Rev. D **53**, 6565 (1996) Erratum: [Phys. Rev. D **56**, 4424 (1997)]
doi:10.1103/PhysRevD.53.6565, 10.1103/PhysRevD.56.4424 [hep-ph/9512396].
- [19] U. Chattopadhyay and P. Nath, Phys. Rev. D **53**, 1648 (1996)
doi:10.1103/PhysRevD.53.1648 [hep-ph/9507386].
- [20] J. L. Lopez, D. V. Nanopoulos and X. Wang, Phys. Rev. D **49**, 366 (1994)
doi:10.1103/PhysRevD.49.366 [hep-ph/9308336].
- [21] F. Jegerlehner and A. Nyffeler, Phys. Rept. **477**, 1 (2009) doi:10.1016/j.physrep.2009.04.003
[arXiv:0902.3360 [hep-ph]].
- [22] The ATLAS collaboration [ATLAS Collaboration], ATLAS-CONF-2017-039.
- [23] A. M. Sirunyan *et al.* [CMS Collaboration], arXiv:1709.05406 [hep-ex].
- [24] A. Mustafayev and X. Tata, Indian J. Phys. **88** (2014) 991 doi:10.1007/s12648-014-0504-8
[arXiv:1404.1386 [hep-ph]].
- [25] C. S. Ün, Ş. H. Tanyıldızı, S. Kerman and L. Solmaz, Phys. Rev. D **91**, no. 10, 105033
(2015) [arXiv:1412.1440 [hep-ph]].
- [26] U. Chattopadhyay and A. Dey, JHEP **1610**, 027 (2016) doi:10.1007/JHEP10(2016)027
[arXiv:1604.06367 [hep-ph]].
- [27] G. G. Ross, K. Schmidt-Hoberg and F. Staub, Phys. Lett. B **759**, 110 (2016)
doi:10.1016/j.physletb.2016.05.053 [arXiv:1603.09347 [hep-ph]].
- [28] G. G. Ross, K. Schmidt-Hoberg and F. Staub, JHEP **1703**, 021 (2017)
doi:10.1007/JHEP03(2017)021 [arXiv:1701.03480 [hep-ph]].
- [29] J. A. Casas, A. Lleyda and C. Munoz, Nucl. Phys. B **471**, 3 (1996)
doi:10.1016/0550-3213(96)00194-0 [hep-ph/9507294].
- [30] C. Le Mouel, Phys. Rev. D **64**, 075009 (2001) doi:10.1103/PhysRevD.64.075009
[hep-ph/0103341].
- [31] C. Le Mouel, Nucl. Phys. B **607**, 38 (2001) doi:10.1016/S0550-3213(01)00172-9
[hep-ph/0101351].
- [32] L. Alvarez-Gaume, J. Polchinski and M. B. Wise, Nucl. Phys. B **221**, 495 (1983).
doi:10.1016/0550-3213(83)90591-6
- [33] J. F. Gunion, H. E. Haber and M. Sher, Nucl. Phys. B **306**, 1 (1988).
doi:10.1016/0550-3213(88)90168-X
- [34] A. Strumia, Nucl. Phys. B **482**, 24 (1996) doi:10.1016/S0550-3213(96)00554-8
[hep-ph/9604417].

- [35] H. Baer, M. Brhlik and D. Castano, Phys. Rev. D **54**, 6944 (1996)
doi:10.1103/PhysRevD.54.6944 [hep-ph/9607465].
- [36] S. A. Abel and C. A. Savoy, Phys. Lett. B **444**, 119 (1998)
doi:10.1016/S0370-2693(98)01362-8 [hep-ph/9809498].
- [37] S. Abel and T. Falk, Phys. Lett. B **444**, 427 (1998) doi:10.1016/S0370-2693(98)01401-4
[hep-ph/9810297].
- [38] P. M. Ferreira, hep-ph/0406234.
- [39] M. Brhlik, Nucl. Phys. Proc. Suppl. **101**, 395 (2001). doi:10.1016/S0920-5632(01)01525-0
- [40] P. M. Ferreira, Phys. Lett. B **509**, 120 (2001) Erratum: [Phys. Lett. B **518**, 333 (2001)]
doi:10.1016/S0370-2693(01)01029-2, 10.1016/S0370-2693(01)00552-4 [hep-ph/0008115].
- [41] A. J. Bordner, hep-ph/9506409.
- [42] D. G. Cerdeno, E. Gabrielli, M. E. Gomez and C. Munoz, JHEP **0306**, 030 (2003)
doi:10.1088/1126-6708/2003/06/030 [hep-ph/0304115].
- [43] U. Chattopadhyay and A. Dey, JHEP **1411**, 161 (2014) doi:10.1007/JHEP11(2014)161
[arXiv:1409.0611 [hep-ph]].
- [44] D. Chowdhury, R. M. Godbole, K. A. Mohan and S. K. Vempati, JHEP **1402**, 110 (2014)
doi:10.1007/JHEP02(2014)110 [arXiv:1310.1932 [hep-ph]].
- [45] A. Riotto and E. Roulet, Phys. Lett. B **377**, 60 (1996) doi:10.1016/0370-2693(96)00313-9
[hep-ph/9512401].
- [46] T. Falk, K. A. Olive, L. Roszkowski, A. Singh and M. Srednicki, Phys. Lett. B **396**, 50
(1997) doi:10.1016/S0370-2693(97)00035-X [hep-ph/9611325].
- [47] A. Kusenko, P. Langacker and G. Segre, Phys. Rev. D **54**, 5824 (1996)
doi:10.1103/PhysRevD.54.5824 [hep-ph/9602414].
- [48] A. Kusenko and P. Langacker, Phys. Lett. B **391**, 29 (1997)
doi:10.1016/S0370-2693(96)01470-0 [hep-ph/9608340].
- [49] A. Kusenko, Nucl. Phys. Proc. Suppl. **52A**, 67 (1997) doi:10.1016/S0920-5632(96)00535-X
[hep-ph/9607287].
- [50] A. Kusenko, Phys. Lett. B **358**, 51 (1995) doi:10.1016/0370-2693(95)00994-V
[hep-ph/9504418].
- [51] R. H. Brandenberger, Rev. Mod. Phys. **57**, 1 (1985). doi:10.1103/RevModPhys.57.1
- [52] U. Ellwanger and C. Hugonie, Phys. Lett. B **457** (1999) 299
doi:10.1016/S0370-2693(99)00546-8 [hep-ph/9902401].

- [53] J. E. Camargo-Molina, B. O’Leary, W. Porod and F. Staub, JHEP **1312** (2013) 103 doi:10.1007/JHEP12(2013)103 [arXiv:1309.7212 [hep-ph]].
- [54] J. E. Camargo-Molina, B. Garbrecht, B. O’Leary, W. Porod and F. Staub, Phys. Lett. B **737**, 156 (2014) doi:10.1016/j.physletb.2014.08.036 [arXiv:1405.7376 [hep-ph]].
- [55] M. Bobrowski, G. Chalons, W. G. Hollik and U. Nierste, Phys. Rev. D **90** (2014) no.3, 035025 Erratum: [Phys. Rev. D **92** (2015) no.5, 059901] doi:10.1103/PhysRevD.90.035025, 10.1103/PhysRevD.92.059901 [arXiv:1407.2814 [hep-ph]].
- [56] W. G. Hollik, Phys. Lett. B **752** (2016) 7 doi:10.1016/j.physletb.2015.11.028 [arXiv:1508.07201 [hep-ph]].
- [57] W. G. Hollik, JHEP **1608** (2016) 126 doi:10.1007/JHEP08(2016)126 [arXiv:1606.08356 [hep-ph]].
- [58] J. Beuria, U. Chattopadhyay, A. Datta and A. Dey, arXiv:1612.06803 [hep-ph].
- [59] M. E. Krauss, T. Opferkuch and F. Staub, Eur. Phys. J. C **77** (2017) no.5, 331 doi:10.1140/epjc/s10052-017-4908-4 [arXiv:1703.05329 [hep-ph]].
- [60] J. Beuria and A. Datta, arXiv:1705.08208 [hep-ph].
- [61] J. E. Camargo-Molina, B. O’Leary, W. Porod and F. Staub, Eur. Phys. J. C **73**, no. 10, 2588 (2013) doi:10.1140/epjc/s10052-013-2588-2 [arXiv:1307.1477 [hep-ph]].
- [62] C. L. Wainwright, Comput. Phys. Commun. **183**, 2006 (2012) doi:10.1016/j.cpc.2012.04.004 [arXiv:1109.4189 [hep-ph]].
- [63] L. Girardello and M. T. Grisaru, Nucl. Phys. B **194**, 65 (1982).
- [64] S. P. Martin, Phys. Rev. D **61**, 035004 (2000) [hep-ph/9907550].
- [65] H. E. Haber and J. D. Mason, Phys. Rev. D **77**, 115011 (2008) [arXiv:0711.2890 [hep-ph]].
- [66] J. Bagger and E. Poppitz, Phys. Rev. Lett. **71**, 2380 (1993) [hep-ph/9307317].
- [67] U. Ellwanger, Phys. Lett. B **133**, 187 (1983).
- [68] I. Jack and D. R. T. Jones, Phys. Lett. B **457**, 101 (1999) [hep-ph/9903365].
- [69] J. M. Frere, M. V. Libanov and S. V. Troitsky, Phys. Lett. B **479**, 343 (2000) [hep-ph/9912204].
- [70] S. P. Martin, Phys. Rev. D **92**, no. 3, 035004 (2015) [arXiv:1506.02105 [hep-ph]].
- [71] I. Jack and D. R. T. Jones, Phys. Rev. D **61**, 095002 (2000) [hep-ph/9909570].
- [72] J. P. J. Hetherington, JHEP **0110**, 024 (2001) [hep-ph/0108206].
- [73] I. Jack, D. R. T. Jones and A. F. Kord, Phys. Lett. B **588**, 127 (2004) [hep-ph/0402045].
- [74] M. A. Cakir, S. Mutlu and L. Solmaz, Phys. Rev. D **71**, 115005 (2005) [hep-ph/0501286].

- [75] A. Sabanci, A. Hayreter and L. Solmaz, Phys. Lett. B **661**, 154 (2008) [arXiv:0801.2029 [hep-ph]].
- [76] E. Cincioglu, A. Hayreter, A. Sabanci and L. Solmaz, arXiv:0905.0726 [hep-ph].
- [77] T. Hambye, E. Ma and U. Sarkar, Nucl. Phys. B **590**, 429 (2000) [hep-ph/0006173];
- [78] J. Chakraborty and S. Roy, Phys. Rev. D **85**, 035014 (2012) [arXiv:1104.1387 [hep-ph]].
- [79] M. Quiros, hep-ph/9901312.
- [80] S. P. Martin, Phys. Rev. D **90**, no. 1, 016013 (2014) doi:10.1103/PhysRevD.90.016013 [arXiv:1406.2355 [hep-ph]].
- [81] A. Brignole, J. R. Espinosa, M. Quiros and F. Zwirner, Phys. Lett. B **324**, 181 (1994) doi:10.1016/0370-2693(94)90405-7 [hep-ph/9312296].
- [82] D. M. Pierce, J. A. Bagger, K. T. Matchev and R. -j. Zhang, Nucl. Phys. B **491**, 3 (1997) [hep-ph/9606211].
- [83] F. Staub, Comput. Phys. Commun. **184**, 1792 (2013) doi:10.1016/j.cpc.2013.02.019 [arXiv:1207.0906 [hep-ph]].
- [84] F. Staub, Comput. Phys. Commun. **185**, 1773 (2014) doi:10.1016/j.cpc.2014.02.018 [arXiv:1309.7223 [hep-ph]].
- [85] F. Staub, PoS CORFU **2015**, 027 (2016) [arXiv:1509.07061 [hep-ph]].
- [86] F. Staub, PoS CORFU **2015**, 058 (2016) [arXiv:1603.05958 [hep-ph]].
- [87] W. Porod, Comput. Phys. Commun. **153**, 275 (2003) doi:10.1016/S0010-4655(03)00222-4 [hep-ph/0301101].
- [88] F. Staub, Comput. Phys. Commun. **181**, 1077 (2010) doi:10.1016/j.cpc.2010.01.011 [arXiv:0909.2863 [hep-ph]].
- [89] F. Staub, Comput. Phys. Commun. **182**, 808 (2011) doi:10.1016/j.cpc.2010.11.030 [arXiv:1002.0840 [hep-ph]].
- [90] W. Porod and F. Staub, Comput. Phys. Commun. **183**, 2458 (2012) doi:10.1016/j.cpc.2012.05.021 [arXiv:1104.1573 [hep-ph]].
- [91] W. Porod, F. Staub and A. Vicente, Eur. Phys. J. C **74**, no. 8, 2992 (2014) doi:10.1140/epjc/s10052-014-2992-2 [arXiv:1405.1434 [hep-ph]].
- [92] M. D. Goodsell, K. Nickel and F. Staub, Eur. Phys. J. C **75** (2015) no.1, 32 doi:10.1140/epjc/s10052-014-3247-y [arXiv:1411.0675 [hep-ph]].
- [93] M. Goodsell, K. Nickel and F. Staub, Eur. Phys. J. C **75** (2015) no.6, 290 doi:10.1140/epjc/s10052-015-3494-6 [arXiv:1503.03098 [hep-ph]].

- [94] H. E. Haber and R. Hempfling, Phys. Rev. Lett. **66**, 1815 (1991).
doi:10.1103/PhysRevLett.66.1815
- [95] T. Ibrahim and P. Nath, Phys. Rev. D **63**, 035009 (2001) doi:10.1103/PhysRevD.63.035009 [hep-ph/0008237].
- [96] G. Degrandi, S. Heinemeyer, W. Hollik, P. Slavich and G. Weiglein, Eur. Phys. J. C **28**, 133 (2003) doi:10.1140/epjc/s2003-01152-2 [hep-ph/0212020].
- [97] B. C. Allanach, A. Djouadi, J. L. Kneur, W. Porod and P. Slavich, JHEP **0409**, 044 (2004) doi:10.1088/1126-6708/2004/09/044 [hep-ph/0406166].
- [98] S. P. Martin, Phys. Rev. D **75**, 055005 (2007) doi:10.1103/PhysRevD.75.055005 [hep-ph/0701051].
- [99] R. V. Harlander, P. Kant, L. Mihaila and M. Steinhauser, Phys. Rev. Lett. **100**, 191602 (2008) [Phys. Rev. Lett. **101**, 039901 (2008)] doi:10.1103/PhysRevLett.101.039901, 10.1103/PhysRevLett.100.191602 [arXiv:0803.0672 [hep-ph]].
- [100] S. Heinemeyer, O. Stal and G. Weiglein, Phys. Lett. B **710**, 201 (2012) doi:10.1016/j.physletb.2012.02.084 [arXiv:1112.3026 [hep-ph]].
- [101] A. Arbey, M. Battaglia, A. Djouadi and F. Mahmoudi, JHEP **1209**, 107 (2012) doi:10.1007/JHEP09(2012)107 [arXiv:1207.1348 [hep-ph]].
- [102] M. Chakraborti, U. Chattopadhyay and R. M. Godbole, Phys. Rev. D **87**, no. 3, 035022 (2013) doi:10.1103/PhysRevD.87.035022 [arXiv:1211.1549 [hep-ph]].